Bioresource Technology 425 (2025) 132336

Contents lists available at ScienceDirect

Bioresource Technology

journal homepage: www.elsevier.com/locate/biortech

Multifactorial interaction and influence of culture conditions on yellow fluorescent protein production in *Phaeodactylum tricornutum*

Arun Augustine [a], Anis Messaabi [a], Elisa Fantino [a,b], Natacha Merindol [a], Fatma Meddeb-Mouelhi [a,b], Isabel Desgagné-Penix [a,b,*]

[a] Department of Chemistry, Biochemistry and Physics, Université du Québec à Trois-Rivières, 3351 boulevard des Forges, Trois-Rivières, QC G9A 5H7, Canada
[b] Plant Biology Research Group, Université du Québec à Trois-Rivières, Trois-Rivières, Québec, Canada

HIGHLIGHTS

- Bioengineered P. tricornutum expressing yellow fluorescent protein extrachromosomally.
- A model was developed to predict culture parameters on YFP production in P. tricornutum.
- Optimized conditions increased YFP fluorescence and yield by 4.2x and 1.8x, respectively.
- Inhibition of the ubiquitin–proteasome system increased YFP levels by 50–150 % after 4–8 h.
- Cycloheximide treatment significantly reduced YFP stability at 20 h.

GRAPHICAL ABSTRACT

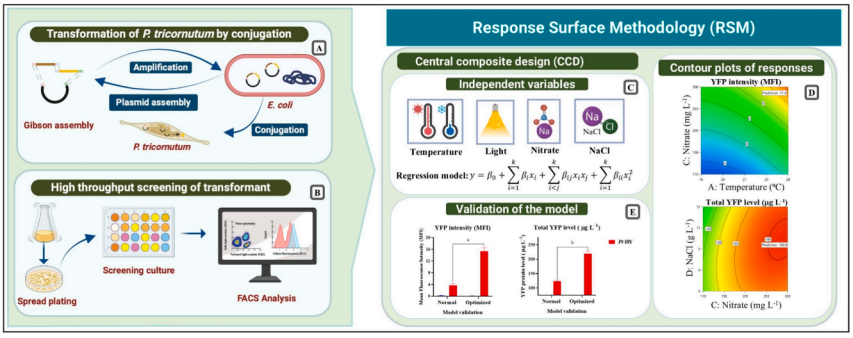

ARTICLE INFO

Keywords:
Microalgae
Genetic engineering
Response surface methodology
Diatoms
Protein inhibitors

ABSTRACT

Phaeodactylum tricornutum is a promising host for light-driven synthesis of heterologous proteins. However, the marine cold-water environment and alkaline-acidic pH shifts in the culture, necessitated by the diatom's growth requirements. In this study, we analyzed the influence of growth condition on maturation and dynamics of the yellow fluorescent protein (YFP) in episomal-transformant *P. tricornutum*. A mathematical model was developed to detect the parameters that affect biomass and YFP production. Optimized conditions increased YFP mean fluorescence intensity (MFI) per cell by 4.2-fold (3.6 ± 0.6 to 15.4 ± 1.1) and total protein levels in the culture by 1.8-fold (123 ± 4 to 219 ± 9 µg L^{-1}), without affecting biomass. YFP stability studies in P. tricornutum showed that the ubiquitin–proteasome system contributes the degradation of the recombinant protein, whereas newly synthesized YFP remains stable for up to 12 h. This optimization provides insights into the fluorescent protein-based heterologous production in diatoms.

1. Introduction

Diatoms are major primary producers of the ocean and are considered natural cell factories for high value metabolites, such as pigments, polyunsaturated fatty acids, and terpenoids (Chen et al., 2022). Recent advances in genome sequencing, annotation (Filloramo

* Corresponding author.
E-mail address: Isabel.Desgagne-Penix@uqtr.ca (I. Desgagné-Penix).

https://doi.org/10.1016/j.biortech.2025.132336
Received 28 November 2024; Received in revised form 2 March 2025; Accepted 2 March 2025
Available online 3 March 2025

et al., 2021), and editing tools have increased our ability to harness their potential. *P. tricornutum* is a cold-water obligate photoautotroph with a maximum growth rate at 20 ± 2°C (De Martino et al., 2011). This diatom has been investigated for diverse biotechnological applications, particularly for the light-driven production of biopharmaceutical specialized metabolites (Fantino et al., 2024). It exhibits a poorly silicified frustules, which reduces the transformation barrier (Karas et al., 2015), and a rapid growth rate under diverse environmental conditions. However, the efficacy of this heterologous production platform is strongly influenced by environmental factors such as temperature, salinity, light intensity, CO_2 supplementation, and silicate concentration (De Martino et al., 2011; Gómez-Loredo et al., 2016; Liang et al., 2014).

To overcome photoinhibition and achieve maximum biomass production, the light intensity must be optimized based on the cell density, culture volume, and surface area (Sivakaminathan et al., 2018). Nitrogen, as a building block for biomolecules synthesis, is the most important macronutrient for algal growth. Higher levels increase algal growth and metabolism, while nitrate-deficiency leads to reduced biosynthesis and increases recycling of amino acids, proteins, and nucleic acids (Alipanah et al., 2015). Phosphate is also essential to the diatom growth, as a key component of membrane phospholipids. A deficiency causes the downregulation of processes like photosynthesis, ribosome and nucleic acid biosynthesis, and of nitrogen assimilation (Alipanah et al., 2018). The concentration of micronutrients such as vitamins and metal ions in the medium play a crucial role in determining the growth of algae as well (Ouyang et al., 2018).

In addition to environmental and culture factors, recombinant protein turnover and maturation process also depend on the nature of the promoter and the cell division rate (Guerra et al., 2022). The recently reported endogenous highly abundant secreted protein 1 (HASP1) promoter strongly and constitutively expresses heterologous genes of interest in *P. tricornutum* at all growth phases, especially in the stationary phase when the culture reaches maximum biomass (Erdene-Ochir et al., 2019), attracting the interest of researchers (Slattery et al., 2022).

Several fluorescent proteins (FPs) have been used in the diatom to gain insight of various cellular dynamics and processes, facilitate screening, monitor recombinant gene expression, and measure protein turnover (Diamond et al., 2023; Fantino et al., 2024). FPs must undergo an autocatalytic process of maturation, which includes various folding and post-translational modifications that result in the formation of a functional chromophore and fluorescence emission (Guerra et al., 2022). The kinetics of this process are influenced by environmental factors such as molecular oxygen, temperature, pH, and chloride ion (Cl^-), and impacts on the accuracy of dynamic measurements and *in vivo* fluorescence intensity.

Systematic characterization and screening of *P. tricornutum* culture parameters for optimal growth and FP accumulation would be highly valuable to help researchers select the optimum conditions for heterologous protein production To monitor the impact of culture parameters on growth, fluorescence formation, and heterologous protein production in *P. tricornutum*, we used transconjugants lines carrying the yellow FP (YFP), and applied a strategic Plackett-Burman design (PBD) as well as a central composite design (CCD) (Rajendran et al., 2008). YFP has been frequently used in *P. tricornutum* studies, displays a high pKa, extinction coefficient, and relatively bright fluorescence compared to other FPs (Marter et al., 2020), and mathematical models such as the response surface methodology (RSM) allows for the evaluation of the interactions between multiple factors influencing protein expression.

This study mainly focused on: (1) generating a transgenic line of *P. tricornutum* with an episomal vector carrying the *yfp* gene under the HASP1 promoter and evaluating the expression, protein production, and chromophore formation under varying culture conditions; (2) screening for factors impacting YFP production; (3) optimizing the culture conditions for maximum growth, maturation, and total YFP production; and (4) assessing the stability of YFP *in silico* and in *P. tricornutum* cells using proteasome and protein synthesis inhibitors.

2. Materials and methods

2.1. Diatom growth and culture conditions

P. tricornutum Bohlin strain (Culture Collection of Algae and Protozoa CCAP 1055/1) was maintained in an algal growth chamber at 18 ± 1°C, 75 µmol m^{-2} s^{-1}, pH 8.0 ± 0.5 with a 16:8h light/dark photoperiod and continuous orbital shaking at 130 rpm (Innova S44i, Eppendorf) in modified L1 media with 150 mg L^{-1} of $NaNO_3$ and 10 mg L^{-1} of $NaH_2PO_4H_2O$ (Slattery et al., 2022). All algal experiments were conducted in 250 mL conical flasks in batch culture mode. The optical density was measured at OD_{680} using a microplate reader (Synergy H1, BioTek), and the dry cell weight of *P. tricornutum* was calculated from the regression graph built against OD_{680} versus the dried algal biomass (40 mL culture) and expressed in terms of g L^{-1}.

2.2. Generation of P. Tricornutum transconjugants

Plasmid DNA constructs were constructed using Gibson assembly as described by Diamond et al. (2023). Empty vector (EV) carrying the antibiotic selection marker gene *N-acetyltransferase* (*nat*) against nourseothricin (NTC) under the FcpC promoter and terminator in pPtGE30 was used as a negative control. The other episome carried *YFP* under the HASP1 promoter and FcpA terminator by replacing the UR3 region of the EV backbone (Fig. 1 and (see supplementary material)) tagged with 3HA at the C-terminal.

Transgenic lines of *P. tricornutum* were obtained by conjugation as described by Karas et al. (2015). The positive transformants carrying the recombinant plasmid started to form colonies on the NTC plate after a two-week period. Positive transformants were screened, as described in (Diamond et al., 2023). YFP fluorescence from *P. tricornutum*-positive transformants was assessed using the microplate reader. The cell culture (200 µL) was measured for fluorescence in black 96 well plates at Ex/Em wavelengths of 500/531 nm (n = 3). Strains containing plasmids YFP (16,168 bp) and EV (14,530 bp) are referred to here as *Pt*-HY and *Pt*-EV, respectively.

2.3. Fluorescence-activated cell sorting of bioengineered P. Tricornutum

P. tricornutum transconjugants were sorted by YFP production using a FACSMelody™ (BD bioscience, USA). The screened *P. tricornutum* transconjugants were grown in L1 liquid media with appropriate antibiotics in log phase (14 days) and used for the first sorting. Culture preparation, gating strategy and singlet selection were performed as in Diamond et al. (2023). YFP was analyzed on a 527/32 nm bandpass filter channel. Sorted cells were collected in an Eppendorf tube containing 0.5 mL L1 media without antibiotics, centrifuged at a low speed of 3500 *g* for 10 min. The resulting cell pellet was resuspended in fresh L1 medium supplemented with NTC 100 µg mL^{-1} and chloramphenicol 25 µg mL^{-1}. For the initial screening, 30 positive transconjugants per construct were screened based on antibiotic selection (*Pt*-EV) and YFP fluorescence (*Pt*-HY). *P. tricornutum* transconjugants with higher mean YFP fluorescence intensity (MFI) were used for full-scale experiments. *Pt*-EV transformants were used as negative controls to deduce spillover YFP autofluorescence signals during the screening process. (Diamond et al., 2023).

2.3.1. Whole-cell YFP fluorescence measurements by flow cytometry

Cytometry was performed on a Cytomics FC 500 flow cytometer (Beckman Coulter) equipped with Argon (488 nm) and HeNe (633 nm) lasers. Only the *P. tricornutum* population with homogenous cell size and chlorophyll autofluorescence level was considered in the analysis to exclude cell debris and other background noise. A least 20,000 gated cells were analyzed for each sample. The inherent properties of the cells and other characteristics of heterologous fluorescence properties (MFI, % of YFP^+ cells, and cell size variations in the culture) were analyzed

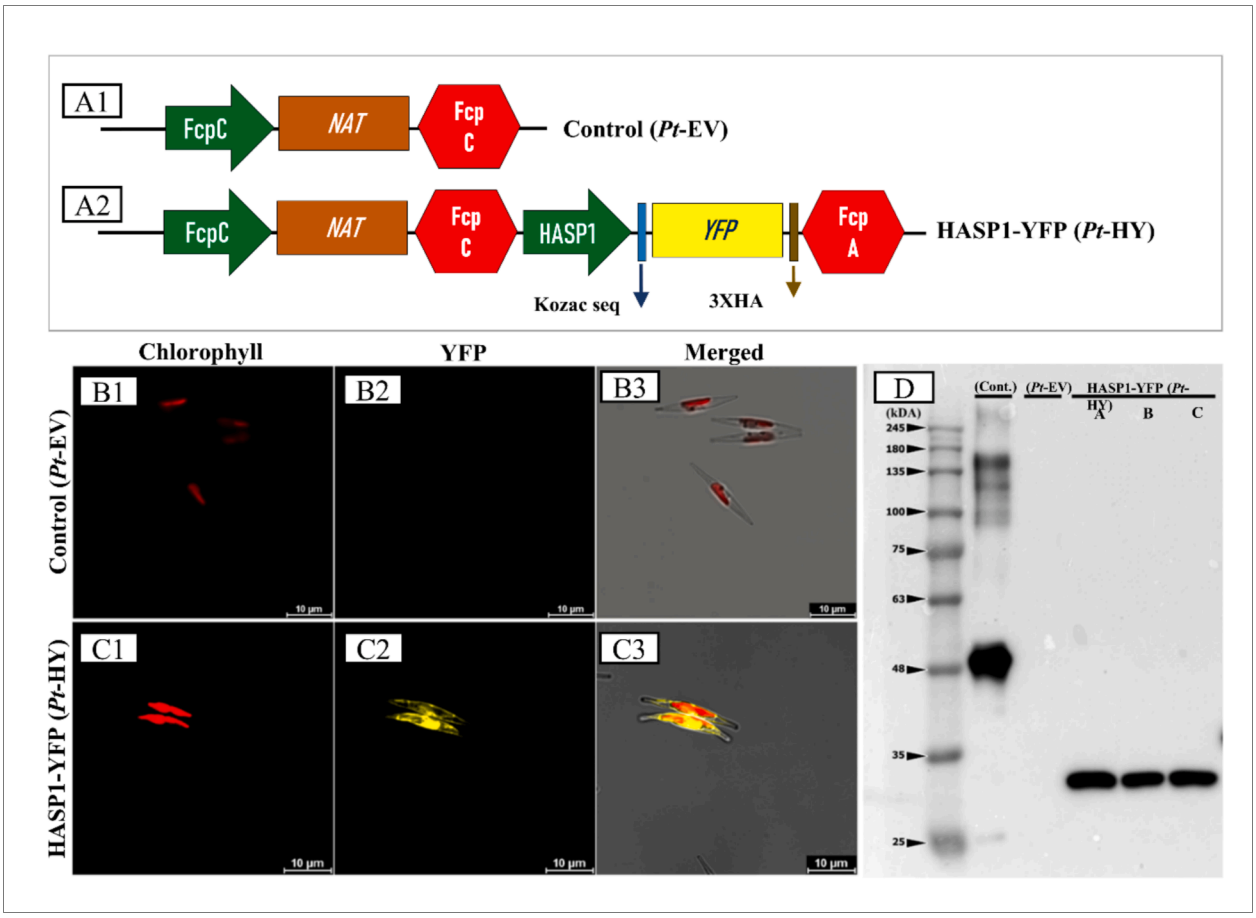

Fig. 1. *P. tricornutum* episomal transconjugants accumulate yellow fluorescent protein. (A) Schematic overview of constitutive vector circuit design. (A1) Synthetic module showing the *nat* gene under the constitutive FcpC promoter and terminator (*Pt*-EV). (A2) The construct with the antibiotic-resistant gene and *yfp* gene under HASP1 constitutive promoter and FcpA terminator (*Pt*-HY). (B and C) *In vivo* subcellular localization of YFP in *Pt*-EV and *Pt*-HY, respectively, by confocal microscopy. (B1 and C1) Chlorophyll fluorescence is shown as red signal. (B2 and C2) YFP fluorescence is shown as yellow signal. (B3 and C3) The overlay of the two signals. The scale bars represent 10 µm. (D) Western blot analysis showing YFP detection (YFP:3HA; 32 kDa) in the transformed *Pt*-HY cells using an anti-HA antibody. *Pt*-EV was used as control.

using FlowJo version 10.8 software (BD Biosciences, USA) (Diamond et al., 2023).

2.4. Subcellular localization of YFP

Transconjugant *P. tricornutum* cells were visualized using a confocal microscope under a 40x objective lenses (Leica M165 FC Fluorescent Stereo Microscope). The *in vivo* localization of YFP in the transformed cells was performed in an 8-day-old culture. YFP, chlorophyll, and propidium iodide (PI, Sigma Aldrich) were excited at 488 nm and detected using YFP (520–535 nm), PI (610–620 nm), and RFP (625–720 nm) filters, respectively, as in Diamond et al. (2023).

2.5. Total RNA extraction and qPCR-based quantification of YFP

Total RNA was isolated from the transformed *P. tricornutum* biomass (15 mL of 8-day-old culture). The algal pellets were collected by centrifugation at 4000 rpm for 5 min at 4 °C and flash frozen in liquid nitrogen, was stored at −80 °C for later extraction using the RNeasy Plant Mini Kit, according to the manufacturer's protocol (QIAGEN). RNA quality and quantity were confirmed using an Implen NanoPhotometer®. Real-time qPCR analysis was performed using the Luna® Universal One-Step RT-qPCR Kit according to the manufacturer's instructions (New England Biolabs). Amplification and relative quantification were performed in triplicate using antibiotic (*nat*) and *YFP* specific primers (see supplementary material), on a CFX-connected Real-Time PCR System (Bio-Rad). Primer specificity was verified by analyzing the melting curves. Data processing and statistical analysis were performed using the CFX Maestro software (Bio-Rad, USA). The relative expression of all genes was calculated by the $2^{-\Delta\Delta CT}$ method (Pfaffl, 2001) using *P. tricornutum Tuba* (Tubulin alpha) and *EF1α* (Elongation factor alpha) as the endogenous reference genes (Siaut et al., 2007).

2.6. Protein extraction

P. tricornutum culture was centrifuged (20 mL) at 4000 g for 10 min at 4 °C. The pellet was re-suspended in solubilization buffer at a ratio of 100 mg mL^{-1} (0.75 mM SDS, 10 % glycerol, 51.4 mM Tris HCl pH 8, and 0.02 mM EDTA) of the wet weight and stored samples in −80 °C for further analysis. The pellet was thawed in ice water, and extraction was performed as described in Fantino et al. (2024), and proteins stored at −80 °C for further analysis. Total protein amount was quantified using the RC DC Protein Assay Kit (Bio-Rad) and a linear calibration curve was constructed using Bovine Serum Albumin (BSA) as a protein standard.

2.7. Elisa-based YFP quantification

Quantification of recombinant YFP in *P. tricornutum* total protein extract was performed using a GFP sandwich ELISA (# Cat. No. AKR 121, Cell Biolabs, USA), according to the manufacturer's instructions

starting from, 100 µL of total protein per well (1 µg) extracted from the transformed *P. tricornutum* cell lysate. The color intensity of the solution in each well was read in the microplate reader (OD_{450}). The quantification of YFP in the total protein samples was determined using a standard curve prepared with GFP standard 0–2 ng mL^{-1} included in the kit.

2.8. Western blot detection of YFP in P. Tricornutum transconjugants

The soluble protein fraction (40 µg) of the cell lysate from transgenic *P. tricornutum* cells was loaded onto 12 % SDS-PAGE for western blot detection of heterologous proteins. The transfer into a polyvinylidene fluoride membrane and immunoblotting were performed as described in Fantino et al. (2024). The BLUelf prestained protein ladder was used as the molecular weight marker for comparison (GeneDireX, Cat. No. PM008-0500), and 10 ng of positive-tag control (protein of GenScript Multiple tag M0101) loaded onto the SDS-PAGE gel as a positive control. In all blotting analyses, two gels with identical samples were run in parallel, one used for western blotting and the other for the loading control after staining with Coomassie brilliant blue.

2.9. Plackett-Burman design screening for significant culture conditions for biomass and YFP production

The experiments were performed using L1 medium as the basal medium supplemented with NTC at a concentration of 100 µg•mL^{-1}. Exponentially growing *P. tricornutum* cells were used as the inoculum with initial OD_{680} adjusted to 0.05. The significant variables affecting biomass (OD_{680}) and YFP production (flow cytometry) in *P. tricornutum* were screened using a PB design with Design-Expert® software V 7.0 (Stat-Ease Inc.). Seven culture variables, including temperature, light, $NaNO_3$, NaH_2PO_4, NaCl, metal solution, and vitamin solution, were tested in their upper (+) and lower limits (−) for their influence on biomass or YFP production. A set of 12 different experiments was carried out in triplicate (see supplementary material), and the mean values of biomass, MFI of YFP, and % of YFP^+ cells were considered as a response for screening the significant culture variables (Plackett & Burman, 1946). Responses were analyzed by ANOVA, and variables with a confidence level above 95 % ($p < 0.05$) were considered to have significant effects on biomass, YFP intensity, and % of YFP^+ cells (Rajendran et al., 2008).

2.10. Optimization of culture conditions for biomass and YFP production by response surface Methodology

A 2^4 factorial CCD-based RSM with 30 sets of experiments was used to optimize the level of the significant variables identified from the PB experiments, such as temperature (x_1), light (x_2) nitrate (x_3), and NaCl (x_4) at five different levels. Other parameters, which were less significant, such as phosphate, metal, and vitamin concentrations, were maintained at constant levels as per the standard conditions. The experiments were conducted using exponentially grown diatoms at initial OD_{680} of 0.05 in 250 mL Erlenmeyer flasks containing 50 mL of medium prepared according to the design shown in (see supplementary material).

The relationship between independent variables and responses was calculated using the second-order polynomial equation response (1).

$$y = \beta_0 + \sum_{i=1}^{k} \beta_i x_i + \sum_{i<j}^{k} \beta_{ij} x_i x_j + \sum_{i=1}^{k} \beta_{ii} x_i^2 \quad (1)$$

where y represents the predicted response (biomass, YFP MFI, % of YFP^+ cells, and total YFP level), β_0 is the model constant, β_i is the linear coefficient, β_{ii} is the quadratic coefficient, β_{ij} is the interaction coefficient, and k is the number of factors. The ANOVA for the experimental data and model coefficients were calculated using Design-Expert® software. To visualize the variable interactions and their impact on the response, 2D contour plots were generated.

2.11. Experimental validation of the model and statistical analysis

The statistical model was validated for biomass, YFP MFI, % of YFP^+ cells, and YFP level using the methods described earlier. Experimental values were subsequently compared with model-predicted values and standard culture conditions. All experiments were performed in triplicate (n = 3), and the results are described as mean ± standard deviation (SD), tested with a two-way ANOVA, in which different culture conditions were considered fixed factors and responses as dependent variables. Statistical analyses, such as ANOVA and Student's *t*-test, were performed using GraphPad Prism V8 software. The statistically difference between the control and experiment groups tested using Bonferroni's multiple comparison. A *p*-value < 0.05 was considered statistically significant, and shown as $p < 0.05$(a), $p < 0.005$(b), and $p < 0.0005$(c).

2.12. Protein stability analysis

2.12.1. In silico thermal stability analysis

The thermal stability curve of the YFP was predicted using the protein structure-based melting temperature (*Tm)* prediction tools SCooP v-1.0 (Pucci et al., 2017). The folded structure of YFP was generated using a ColabFold from the amino acid sequence (Mirdita et al., 2022).

2.12.2. In vivo stability analysis of YFP in transformed P. Tricornutum by protein inhibitors

Eight-day-old P. tricornutum cultures (100 mL) grown in optimized conditions with $OD_{680} = 0.6$ in 250 mL conical flasks were used for protein inhibitor treatment, as described by Im et al. (2024). Cultures with equal OD_{680} were treated with 50 µM of the proteasome inhibitor MG132 (MedChemExpress) dissolved in DMSO and/or 100 µM of the protein synthesis inhibitor cycloheximide (CHX) (Sigma-Aldrich) dissolved in water. DMSO was used as solvent control. The samples were harvested at the beginning of the light period (8 am), corresponding to the time of treatment initiation, and then every 4 h for the next 24 h. After the first harvest, the respective inhibitor solutions were added to the cultures (8 am). At each time point, 10 mL of each sample was collected and centrifuged at 4,000 *g* for 10 min at 4 °C and pellets resuspended in 250 µL of solubilization buffer. The pellet storage, protein extraction and western blotting were performed as described in section 2.6 and 2.8 except that the membrane was incubated at room temperature for 1 h with primary mouse YFP antibody (Cedarlane) 1:1000 dilution in TBS-T with 3 % BSA. For immunoblotting of housekeeping proteins, *β*-actin antibody conjugated with HRP (BioLegend) at a 1:20,000 dilution in TBS-T was used. The densiometric analysis of immunoblot was done using ImageJ software v1.54 k. The effect of protein inhibitor treatment on cell viability were visualized by confocal microscopy by PI staining, added to the treated culture at a final concentration of 3 µg mL^{-1} and incubated at room temperature for 30 min (Fantino et al., 2024).

3. Results and discussion

3.1. Growth and YFP production of P. Tricornutum transconjugants

In this study, we used two *P. tricornutum* transconjugant strains, *Pt*-EV (negative control) and *Pt*-HY strains harboring an episomal vector to produce YFP:3HA (Fig. 1A). To maintain high YFP expression, and to mitigate episomal instability and transgene silencing (Diamond et al., 2023), cultures underwent periodic fluorescence-based sorting. Guerra et al. (2022) showed that *in vivo* brightness and fluorescent protein maturation are tightly coupled with cell cycle gene expression, histone-like proteins, and DNA replication in yeast, suggesting that modeling the

culture dynamics and quantification of fluorescence of individual cells requires synchronized sampling. As a result, biomass and fluorescence production were assessed at the end of the light period when *P. tricornutum* cells have completed division and exhibit peak fluorescence (Vartanian et al., 2009). We focused on optimizing growth and heterologous protein production by monitoring *P. tricornutum* cultures until they reached the stationary phase.

YFP fluorescence in *Pt*-HY was confirmed by confocal analysis (Fig. 1B and C), and western blotting (Fig. 1D). A preliminary one-factor-at-a-time analysis (OFAT) analysis assessed the impact of temperature (18, 21, and 24 °C with 75 μmol m^{-2} s^{-1} of light), and light intensity (50, 75, and 100 μmol m^{-2} s^{-1} at 18 °C) on growth and fluorescence production (see supplementary material). Cultures reached stationary phase after 15 days, regardless of the temperature or light conditions Temperature significantly affected early biomass accumulation. At 24 °C compared to 18 °C, growth was reduced at day 5 (p = 0.001; 33 % decrease) and day 8 (p = 0.003; 12 % decrease), but difference was no longer significant from day 10 (p = 0.18), suggesting adaptation mechanisms. The MFI, and % of YFP^+ cells in the culture reached a maximum at day 8 under different temperatures and light intensities (see supplementary material). Then, YFP fluorescence decreased despite higher biomass. This might be due to flow cytometry single cell resolution analysis compared the microplate reader measuring accumulated fluorescence in the well, including proteins secreted in the extracellular media (Erdene-Ochir et al., 2019). Nonetheless, YFP fluorescence was enhanced at 24 °C, with a 13.0 ± 0.7 % increase in the % of YFP^+ cells (p = 0.01) and a 3.2 ± 0.1-fold increase YFP MFI (p = 0.0001), a variable that is proportional to the amount of YFP fluorescence intensity per cell. At that temperature with 75 μmol m^{-2} s^{-1} of light, more than 60 % of the cell population produced a high level of YFP fluorescence until the 15th day, consistently with reports of enhances YFP folding at higher maturation (Iizuka et al., 2011).

Light intensity also influenced growth and fluorescence. Cultures grown with 50 compared to 75μmol m^{-2} s^{-1} of light showed a significant reduction in biomass at day 5 (p = 0.007; 28 % decrease) and the 8th day (p = 0.02; 8.3 % decrease). At day 8, these cultures exhibited showed a 1.4 ± 0.1-fold increase in both MFI (p = 0.01) and a 7.8 ± 3.0 % increase in % of YFP^+ cells (p = 0.001) (see supplementary material). Overall, among the two physical parameters tested, only higher temperatures had a transient impact on biomass in the initial growth phases. Despite variations in growth, MFI and % of YFP^+ cells peaked at day 8 under all conditions, suggesting a stable fluorescence expression pattern. This time point was selected for further optimization experiments.

3.2. Screening for significant factors affecting biomass and YFP production

To optimize YFP production, we used a PB design to evaluate the impact of seven culture factors on biomass, MFI and % of YFP^+ cells. Each factor was investigated experimentally at two levels, as per the PBD model (see supplementary material). The R^2 (coefficient of determination) value determines how well the model fits the experimental data. The regression model showed a high fit for biomass production (R^2 = 0.97), meaning that up to 97 % of the variation could be explained by the model (Table 1). The adjusted R^2 (0.91) was in reasonable agreement with the predicted R^2 of 0.72 (difference < 0.2), and the *F*-value (17.46, p = 0.008) confirmed the model' significance. Similarly, MFI and % of YFP^+ had R^2 values of 0.97 and 0.93, respectively. The adjusted R^2 (0.93) for MFI agreed reasonably well with the predicted R^2 of 0.75 (Table 1). However, the adjusted R^2 (0.79) for the % of YFP^+ cells differed significantly from the predicted R^2 (0.36) (>0.2) (Table 1), suggesting that the model was too simplistic for this outcome. The adequate precision value (7.99 > 4) confirmed that the model provided a good signal-to-noise ratio for exploring the design space. The PB factorial screening revealed that biomass increased with higher nitrate, light intensity, and NaCl concentration, and decreasing temperature (see supplementary material). YFP fluorescence (MFI and % of YFP^+ cells) increased with higher temperature and nitrate concentration (see supplementary material). In contrast with the preliminary OFAT analysis, light was a significant factor for biomass but not for MFI or % of YFP^+ cells, which may be due to interactive effects with other medium components.

Table 1
Regression coefficient and statistical significance of PBD for biomass, MFI, and YFP^+ cells in *P. tricornutum*.

Regression Coefficients	Biomass (g L^{-1})	YFP intensity (MFI)	YFP^+ cells (%)
Model	[a]	[a]	[a]
Intercept	0.58	5.09	54.06
A-Temperature	−0.05[b]	2.56[b]	10.11[a]
B-Light	0.08[b]	0.14	0.42
C-Nitrate	0.08[b]	2.59[b]	17.16[a]
D-Phosphate	0.01	−0.83	−12.76[a]
E-NaCl	0.07[a]	−0.33	−3.81
F-Metal Solution	−0.04	0.73	−5.92
G-Vitamin	0.02	−0.30	6.48
R^2	0.96	0.97	0.92
Adjusted R^2	0.91	0.92	0.79
Predicted R^2	0.71	0.75	0.36
Adeq Precision	11.94	14.55	7.99

P value = < 0.0005[c], < 0.005[b], < 0.05[a].

In summary, temperature, and nitrate significantly affected YFP, while temperature, light, nitrate, and NaCl influenced biomass. Temperature, nitrate, and phosphate significantly modulated the % of YFP^+ cells. Thus, temperature, light, nitrate, and NaCl with significant effects on biomass and YFP production were selected for further optimization using CCD.

3.3. Mathematical modeling and process optimization for biomass and YFP production

RSM was used to evaluate interactions between multiple culture factors, with temperature (A), light (B), nitrate (C), and NaCl (D) chosen based on the PBD responses. In the CCD model, each variable was analyzed at five coded levels (−α, −1, 0, +1, +α) (see supplementary material). Second-order polynomial equations were obtained to describe biomass production, YFP intensity, % of YFP^+ cells, and total YFP level by applying multiple regression analysis to the experimental response data (see supplementary material). The CCD model was highly significant (p < 0.0001) for all responses, with a non-significant lack of fit (Table 2). The *F*-values for biomass, MFI, % of YFP^+ cells, and total YFP were 29.82, 71.18, 88.75, and 16.57, respectively. Among the tested factors, nitrate had the highest regression coefficients (β) for all responses (R1 = 0.08, R2 = 3.10, *R*3 = 11.75, and R4 = 35.73), which represents the mean change of dependent variable given a one-unit shift in an independent variable (Dayana Priyadharshini & Bakthavatsalam, 2016). Temperature had the second highest regression coefficient, while NaCl and light intensity had the lowest β-values for all responses (Table 2). This confirms that nitrate and temperature are the most influential factors for biomass, and YFP production, while NaCl and light had minimal impact, except for NaCl on total YFP yield. The quadratic terms A, B, C, and D and the interactive terms AB, AC, and BD impacted significantly biomass production (Table 2). The model terms A, AC, and BC affected MFI levels, while the % of YFP^+ cells were significantly modulated by B, C, D, AB, and AC. Interestingly, total YFP level measured by ELISA was influenced by C, D, and interactive terms (CD) (Table 2). Overall, these findings suggest that biomass and YFP production were significantly influenced by each independent variable, with noticeable interactions between factors further improving the responses.

Table 2
Regression coefficient and statistical significance of CCD for biomass and YFP production in *P. tricornutum*.

Regression Coefficients	Biomass (g L^{-1})	YFP intensity (MFI)	YFP^+ cells (%)	Total YFP level (µg L^{-1})
Intercept	0.83	5.03	67.53	164.94
A-Temperature	−0.06[c]	1.87[c]	6.99[c]	5.31
B-Light	−0.01	0.02	2.18[c]	−5.51
C-Nitrate	0.08[c]	3.10[c]	11.75[c]	35.73[c]
D-NaCl	−0.01	−0.01	−1.69[b]	−10.37[b]
AB	0.04[b]	0.24	−1.27	−1.75
AC	−0.05[c]	0.35[a]	−5.86[c]	−3.61
AD	0.01	0.02	−1.36[a]	5.18
BC	−0.01	0.37[a]	−0.10	−2.01
BD	−0.03[b]	0.16	−1.01	7.26
CD	0.01	0.25	−0.90	8.55[a]
A^2	−0.05[c]	0.82[c]	−0.94	0.62
B^2	−0.04[c]	−0.03	2.80[c]	1.16
C^2	−0.05[c]	0.15	−5.68[c]	−19.12[c]
D^2	−0.02[b]	−0.04	2.49[c]	−9.69[b]
R^2	0.97	0.99	0.99	0.94
Adjusted R^2	0.93	0.97	0.98	0.88
Predicted R^2	0.83	0.92	0.93	0.70
Adeq Precision	18.29	31.12	38.4	16.89

P value = < 0.0005[c], < 0.005[b], < 0.05[a].

3.3.1. Mutual interactions between the significant factors

3.3.1.1. Interactive factors affecting biomass production in P. Tricornutum. The RSM approach facilitated the identification of the optimal conditions for fluorescence intensity and heterologous protein yield in *P. tricornutum*. The contour plots in Fig. 2 were generated from the experimental responses of biomass as per the CCD model using a second-order polynomial Eq. (1). They were constructed using the variables in the experimental range, while the other factors were maintained at their optimum levels as per the standard culture conditions. Significant interactions for biomass production were observed between temperature (A) vs. light (B) ($p = 0.001$), A vs. nitrate (C) ($p = 0.0001$), and B vs. NaCl (D) ($p = 0.001$), (Fig. 2 A1, A2, A3). As observed following the PB-based screening, an increase in biomass (from 0.5-0.65 g L^{-1}) was observed with increasing nitrate and increasing NaCl concentration (3–18 g L^{-1}), with other medium components temperature (20.5 °C), light (70 µmol·m^{-2}·s^{-1}) and nitrate (188 mg L^{-1}) at central point (see supplementary material). However, the weight of NaCl on biomass production was not significant at higher temperature (24 °C), light intensity (78.2 µmol·m^{-2}·s^{-1}) and nitrate concentration (300 mg L^{-1}) (Fig. 2 A3).

In agreement with the present observation, a salinity study by Liang et al. (2014) in *P. tricornutum* showed maximum photochemical efficiency of PSII (Fv/Fm) and maximal relative electron transport rate (rETRmax) at a salinity of 20–40 practical salinity units (PSU). As temperature and light intensity decreased, biomass increased. The present observation agrees with the previous factorial optimization studies of Nur et al. (2018) and Gómez-Loredo et al. (2016) in *P. tricornutum,* which showed that there was a significant interactive effect between temperature and light intensity on the level of major light-harvesting pigments such as chlorophyll *a* and fucoxanthin. The level of these pigments reduced with increasing light intensity above 120 µmol·m^{-2}·s^{-1}. In contrast, Wu et al. (2010) observed an increase in biomass at higher temperatures and light intensity under high CO_2 levels in the media. This could be due to the downregulation of the carbon concentration mechanism, which serves as an energy sink. As a result, elevated CO_2 levels in the medium reduce non-photochemical quenching and the energy utilized by this process, which ultimately increases the photosynthetic carbon fixation rate. Overall, biomass production was driven by interactions between temperature, light, nitrate, and NaCl, with optimal growth under moderate temperature and light and increased NaCl and nitrate.

3.3.1.2. Interactive factors affecting YFP production in P. Tricornutum. In addition to biomass optimization, the main objective of this study was to maximize the MFI per cell, % of YFP^+ cells, and total YFP level. Temperature and nitrate played a significant role in YFP intensity, and significant interactions were observed between temperature and nitrate ($p = 0.03$), as well as light and nitrate ($p = 0.02$). As per the model prediction, YFP MFI could be increased from 2 to 11.4 by optimizing these significant factors, while keeping other factors at optimum levels (light 78.2 µmol·m^{-2}·s^{-1} and NaCl 8.5 g L^{-1}), (Fig. 2B1 and B2). The interactions between temperature and nitrate ($p = 0.0001$) and between temperature and NaCl ($p = 0.035$) were also significant when monitoring for % of YFP^+ cells in the culture. The % of YFP^+ cells increased from 40 to 74.5 % by optimizing the most significant factors in the model, such as temperature and nitrate, while keeping other factors at optimum (Fig. 2C1 and *C*2). Total YFP level was significantly modulated by nitrate ($p = 0.0001$) and NaCl ($p = 0.003$) concentrations, and a significant interaction was observed between nitrate and NaCl ($p = 0.034$). Total YFP reached a maximum level at high nitrate with NaCl concentration ranging from 8-11 g L^{-1}, while maintaining other factors at optimum level (temperature 24 °C and light 78.2 µmol·m^{-2}·s^{-1}) (Fig. 2D).

In the present study, of the four parameters tested, NaCl had the least significant impact, with the lowest regression coefficients for MFI (β = -0.01) and % of YFP^+ cells (β = -1.69), which may be due to the specific amino acid substitutions F64L, M153T, and V163A of YFP. These substitutions are known to improve maturation without affecting the excitation and emission spectra and display almost equivalent extinction coefficients and fluorescent quantum yields (Nagai et al., 2002). The protonation and Cl^- binding of YFP chromophore are the two main mechanisms that can decrease its absorbance. The above-mentioned mutations decrease the pH sensitivity and remove the Cl^- sensitivity compared to the original YFP (Nagai et al., 2002). Similar observations on photostability and maturation with regards to temperature and Cl^- were reported in previous study of Guerra et al. (2022). Overall, nitrate, temperature, and light were the most interacting elements for MFI and % YFP^+ cells in the culture. Nonetheless, NaCl content also demonstrated a beneficial interaction with nitrate and was a major factor in the total YFP yield.

3.4. Experimental validation of the model

3.4.1. Biomass production in P. Tricornutum

The CCD model-predicted factors and responses for biomass, YFP MFI, % of YFP^+, and YFP production were experimentally validated using the predicted values listed in Table 3. Under optimized conditions (see supplementary material), there were no significant differences in the biomass of *Pt*-EVs compared to the standard condition. However, *Pt*-HY biomass production increased slightly but significantly ($p = 0.04$; Bonferroni's multiple comparisons test) from 0.77 ± 0.03 to 0.82 ± 0.06 g L^{-1}, compared to standard culture conditions (Fig. 2A, Table 3). This significant difference in biomass may be due to changes in the culture conditions that affect differently *Pt*-HY growth. A biomass production of 0.82 ± 0.06 g L^{-1} in the optimized media aligns with the CCD model predicted biomass of value of 0.71 g L^{-1}, validating the model for biomass production. Furthermore, the biomass yield on day 8 was agreed with the previously reported biomass in *P. tricornutum* by Villanova et al. (2021) 0.87 ± 0.08 g L^{-1} (E10 medium) using different media composition. The work also showed that biomass increased by 2.1-fold (up to 1.86 ± 0.10 g L^{-1}) when changing from phototrophic to mixotrophic culture by the addition of glycerol and bicarbonate ($NaHCO_3$) to the E10 media. Enriched E10 medium increased biomass by a factor of 9 (11.55 ± 0.24) in an upscale photobioreactor (Villanova et al., 2021). The present experiment was performed in batch mode in a conical flask

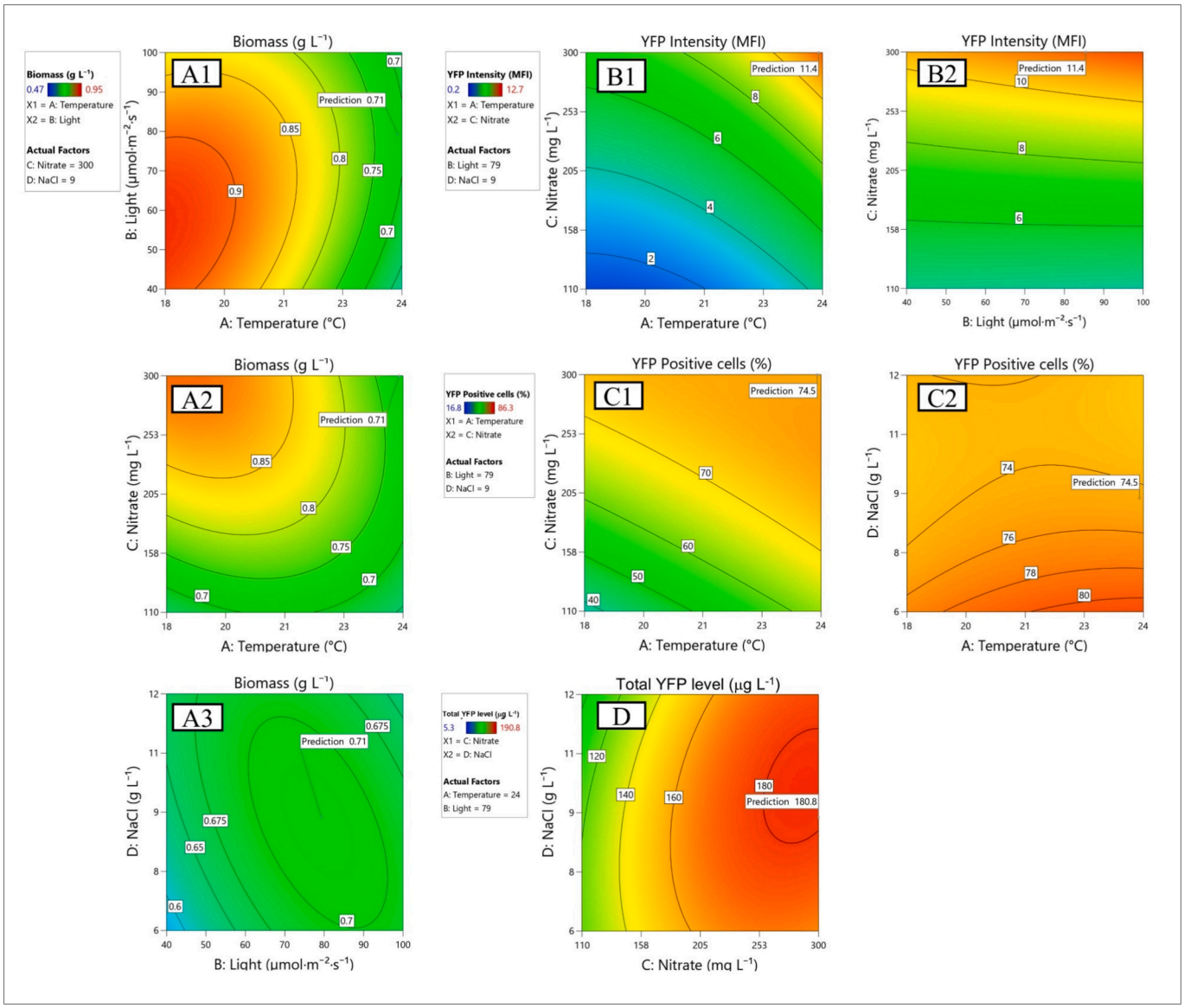

Fig. 2. Contour surface plot of biomass and heterologous yellow fluorescent protein production. (A) The interaction of various culture factors on biomass production. (A1) Temperature (°C) vs light intensity (µmol m^{-2} s^{-1}), (A2) temperature vs nitrate (mg L^{-1}), (A3) light intensity and NaCl (g L^{-1}). (B, C and D) The interaction of various culture conditions on the YFP mean fluorescent intensity (MFI) per cell, the % of YFP^+ cells in the culture population using flow cytometry, and total heterologous protein by ELISA, respectively. (B1 and C1) The interaction of temperature vs nitrate, (B2) light vs nitrate, (C2) temperature vs NaCl, and (D) interaction of nitrate and NaCl on heterologous protein (YFP) level in *P. tricornutum* quantified using ELISA.

using carbon-free L1 media. A further option to boost the biomass and heterologous protein yield in a bioreactor will be to supplement the algal medium with both organic and inorganic carbon sources.

3.4.2. *YFP intensity and percentage of YFP positive cells*

In the present study, under a optimized conditions, MFI increased significantly from 3.6 ± 0.6 to 15.4 ± 1.1 ($p > 0.001$; 4.2-fold increase), and the percentage of YFP^+ cells in *P. tricornutum* culture increased from 49.2 ± 3.5 to 65.5 ± 1.4 % ($p > 0.001$; 16.3 % increase) compared to the standard culture conditions without affecting biomass accumulation (Fig. 3 A, B, C & F and Table 3). This is consistent with previous observations showing that increasing temperature accelerates the maturation of GFP variants (Guerra et al., 2022). Under ideal circumstances, the CCD model projected an MFI of 11.3 and a percentage of YFP^+ cells of 75. The experimental result for MFI (15.4) was greater than the predicted value, indicating that the model was verified. However, % of YFP^+ cells experimental value (65.5) was lower; as a result, the model cannot be verified for this parameter, possibly due to limitations of excitation and detection of this FP by the flow cytometer.

3.4.3. *Heterologous protein production in P. Tricornutum*

In the optimized condition, heterologous protein (YFP) yield increased significantly from 123 ± 4 to 219 ± 9 µg L^{-1} ($p = 0.004$; 1.8 factor increase) compared to standard conditions (Fig. 3 D and Table 3), which corresponded to about 0.2 % of the total soluble protein. As per the CCD model, the independent variables such as increasing nitrate and decreasing NaCl play significant role in improving the total YFP yield. Transcriptome and metabolites studies conducted on *P. tricornutum* by Alipanah et al. (2015) revealed a significant change in gene expression during nitrogen deficiency, reorienting the carbon metabolism toward energy storage mode and increasing the recycling of nitrogen compounds. Erdene-Ochir have reported much higher yield of GFP when its expression was driven by HASP1 promoter (6 mg/L) (Erdene-Ochir et al., 2019). This difference could be due to the relative quantification

Table 3
Experimental validation of CCD model predicted conditions and responses.

Conditions	Standard conditions	Optimized conditions	
	Standard level	Coded levels	Actual levels
Temperature (°C)	18	0.96	23.9
Light ($\mu mol \cdot m^{-2} \cdot s^{-1}$)	75	0.27	78.2
Nitrate (mg L^{-1})	150	1.00	300
NaCl (g L^{-1})	12	−0.16	8.5
Responses	**Experimental value (Std)**	**Predicted Value**	**Experimental Values (Opt)**
Biomass (g L^{-1})	0.77 ± 0.03	0.71	0.82 ± 0.06
YFP intensity (MFI)	3.6 ± 0.6	11.3	15.4 ± 1.1
YFP Positive cells (%)	49.2 ± 3.5	75	65.5 ± 1.4
Total YFP level (μg L^{-1})	123 ± 4	180.2	219 ± 9

$Z = Z^0 - Z^C / \Delta Z$ Where Z and Z^0 indicate coded and real levels of independent variables respectively ΔZ represents the step change while Zc indicates the actual value at central points. Std- standard conditions, Opt- Optimized conditions.

method based on fluorescence intensity rather than on direct protein quantification compared to ELISA. In agreement with our present observation, Kiefer et al. (2022) reported 11.2 μg L^{-1} SARS-CoV-2 spike protein, Chávez et al. (2016) reported 28.0 ± 4.3 μg L^{-1} of human vascular endothelial growth factor and Eichler-Stahlberg et al. (2009) reported 100 μg L^{-1} for human erythropoietin in *Chlamydomonas*. Other studies Ramos-Martinez et al. (2017), reported significantly higher secretory protein yields in mixotrophic green algae, including 15 mg L^{-1} of mVenus. Compared to heterotrophic hosts such as bacteria and yeast, phototrophic systems typically yield lower amount of heterologous protein due to lower biomass production, strong transgene silencing, and protease activity (Ramos-Martinez et al., 2017). These limitations could be overcome through advances in photobioreactor technology and stabilization of heterologous protein using carrier protein or fusion with protease inhibitor or synthetic glycol modules (Ramos-Martinez et al., 2017; Villanova et al., 2021).

The total experimental accumulation of YFP reached 219 ± 9 μg L^{-1}, which was higher than the predicted value of 180.2 μg L^{-1}. Overall, the experimental values were close or above to the predicted response, thus validating the model for all responses except for the percentage of YFP^+ cells. The results also confirm that microalgae are suitable platforms for producing functional proteins in higher yield than plants (Sojikul et al., 2003).

3.4.4. Relative quantification of YFP expression

To determine whether the growth conditions modulated *YFP* transcript levels, as shown by Slattery et al. (2022), we measured the expression of the *yfp* gene in *Pt*-HY and *nat* genes in both strains *Pt*-HY and *Pt*-EV. Although the *nat* gene was driven by the FcpC promoter, the *yfp* gene was expressed under the control of the HASP1 promoter. These mRNA levels were evaluated in an 8-day-old culture in agreement with the highest fluorescence intensity and normalized to *Tuba* and *EF1α* expression. Our results showed that *nat* expression increased under standard conditions compared to optimized conditions in both strains (Fig. 3E). In agreement with MFI and YFP^+ cells % in the population, the relative gene expression of *YFP* was significantly higher ($p < 0.001$, 1.83-fold increase) under optimized conditions, as shown in Fig. 3E. These results highlight the importance of selecting appropriate promoters for multiple genes in the same expression cassette.

3.5. In silico and in vivo stability analysis of YFP in transformed P. Tricornutum.

3.5.1. Structure based thermodynamic stability prediction

We evaluated the intrinsic thermodynamic stability of YFP to understand its folding properties and resistance to denaturation at temperatures used to grow the diatom. Using predictive tools, we assessed key thermodynamic parameters, including *Tm*, which are essential indicators of YFP stability under various environmental conditions (Leuenberger et al., 2017). Protein stability depends on structure, protease activity, host cells, and cellular environment. Dehouck et al. (2008) showed a strong correlation between the T_m value of a protein and the growth temperature of its host. SCooP was recently reported (Pucci et al., 2017) as a protein structure-based protein stability prediction tool, which thermodynamically predicts the protein folding transition by standard free energy $\Delta G(T)$ as a function of temperature (T) when all other parameters (ionic strength, pressure, and pH) are constant. The 3D structure of YFP (Fig. 4A1) was then used to generate the thermodynamic characteristics using the SCooP portal. The YFP T_m was 63 °C, indicating the temperature at which half of the protein population was unfolded. At 21–25 °C, temperature range optimal for *P. tricornutum* growth, the YFP exhibited the most stable folding structure (Fig. 4A2). In agreement with our predicted T_m, Anderson et al. (2023) demonstrated the remarkable thermal stability of mutated YFP variants (Q66E and Q66E + H193Y), showing only a 60 % loss in initial fluorescence after 1 h of exposure at 60 °C. The thermodynamic characteristics of YFP suggests that the observation of the present study relies on host-induced effects rather than inherent fluorescence stability.

3.5.2. In vivo stability of YFP in transformed P. Tricornutum by protein inhibitor treatment

To further elucidate the stability of heterologous proteins in *P. tricornutum*, we studied the turnover and stability of YFP *in vivo*. We investigated the levels and degradation rate of YFP using an immunoblot assay under different treatment conditions. Heterologous protein turnover in cells depends on protein degradation and synthesis. *P. tricornutum* cells were treated with CHX, an antibiotic that inhibits the protein synthesis (Obrig et al., 1971), and MG132, a peptidyl aldehyde that interacts with the 26S proteasome inhibiting ubiquitin-dependent proteasome activity (Lee & Goldberg, 1998)(Fig. 4B1). We evaluated the change in the level of YFP in the presence of MG132, CHX, MG132 + CHX, and control conditions every 4 h for 24 h. (Fig. 4B2).

YFP level was significantly higher after 4 h of treatment with MG132 compared to the control-treated group ($p = 0.01$; 41 % increase), and the same trend was observed following 8 h ($p = 0.05$; 150 % increase) of treatment (Fig. 4B3). The higher accumulation of YFP compared to the control suggests that the recombinant protein was sensitive to 26S proteasomal degradation. MG132 lost its effect on YFP accumulation starting at 12 h and YFP levels were lower than that in the control group after 16 h of treatment. As MG132 is not specifically targeting the recombinant protein, blocking the whole 26S proteasome pathway may lead to interruption of various cellular functions, including cell cycle progression and protein quality (Lee & Goldberg, 1998). Conversely, we observed a steady YFP levels following treatment with CHX for the first 8 h. This suggested that despite the inhibition of protein synthesis, YFP was stable for 8 h in the microalgae. The reduction in the YFP signal compared with the control after 12 h, 16 h, and 20 h of treatment with CHX (significant at 20 h, $p = 0.017$; 88 % decrease) (Fig. 4B3) indicated that intracellular accumulated YFP was being degraded at these timepoints, and is consistent with the reduction of YFP signal following MG132 treatment at these timepoints. After 24 h of treatment, the levels of YFP were comparable to those in control group, implying that the inhibitory effects of both MG132 and CHX were reversible. Inhibitor treatment did not cause any visible change in the culture during the light periods (first 16 h); however, the treated cells started to clump together after the dark cycle (24 h). The level of chlorophyll (Fig. 4D1-4a), YFP^+

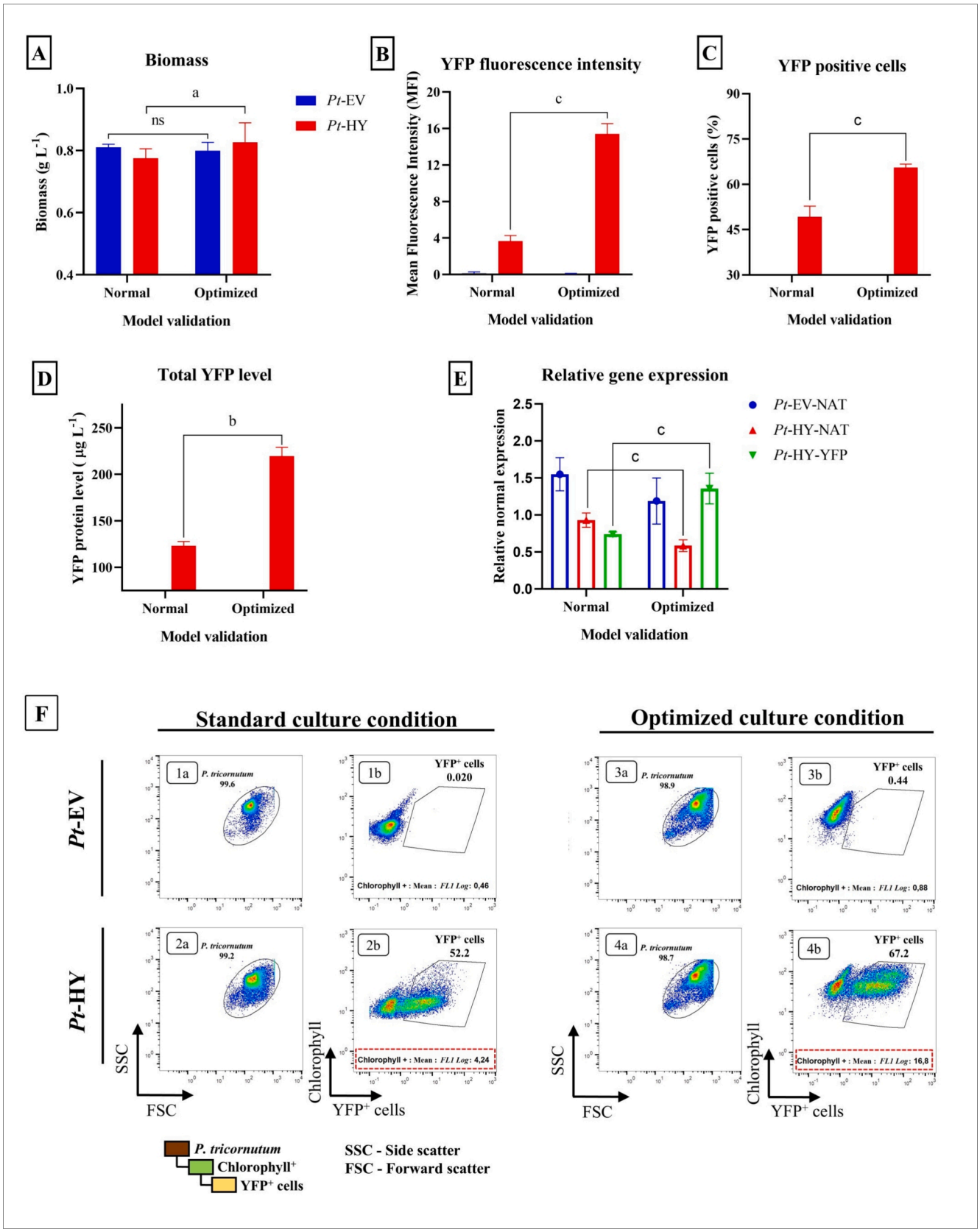

Fig. 3. Experimental validation of the CCD model and compare with standard conditions (A) Biomass accumulation in *Pt*-EV and *Pt*-HY (B and C) YFP MFI and % YFP$^+$ cells quantified using flow cytometry (D) YFP level quantified by ELISA. (E) Relative expression of *yfp* and *nat* gene in *Pt*-EV and *Pt*-HY. The *Pt*-EV-NAT and *Pt*-HY-NAT refers to the analysis of *nat* expression levels in *Pt*-EV and *Pt*-HY, while *Pt*-HY-YFP- refers to *yfp* gene expression levels in *Pt*-HY. (F) Pseudo-color dot plots of *Pt*- EV, and *Pt*-HY (1 and 2) under standard conditions; (3 and 4) under optimized culture conditions. (1b-4b) Pseudo-color dot plots of *Pt*-EV and *Pt*-HY cultures with YFP in the *x*-axis, autofluorescence of chlorophyll on the *y*-axis. The gates of the total YFP$^+$ population were designed according to *Pt*-EV autofluorescence.

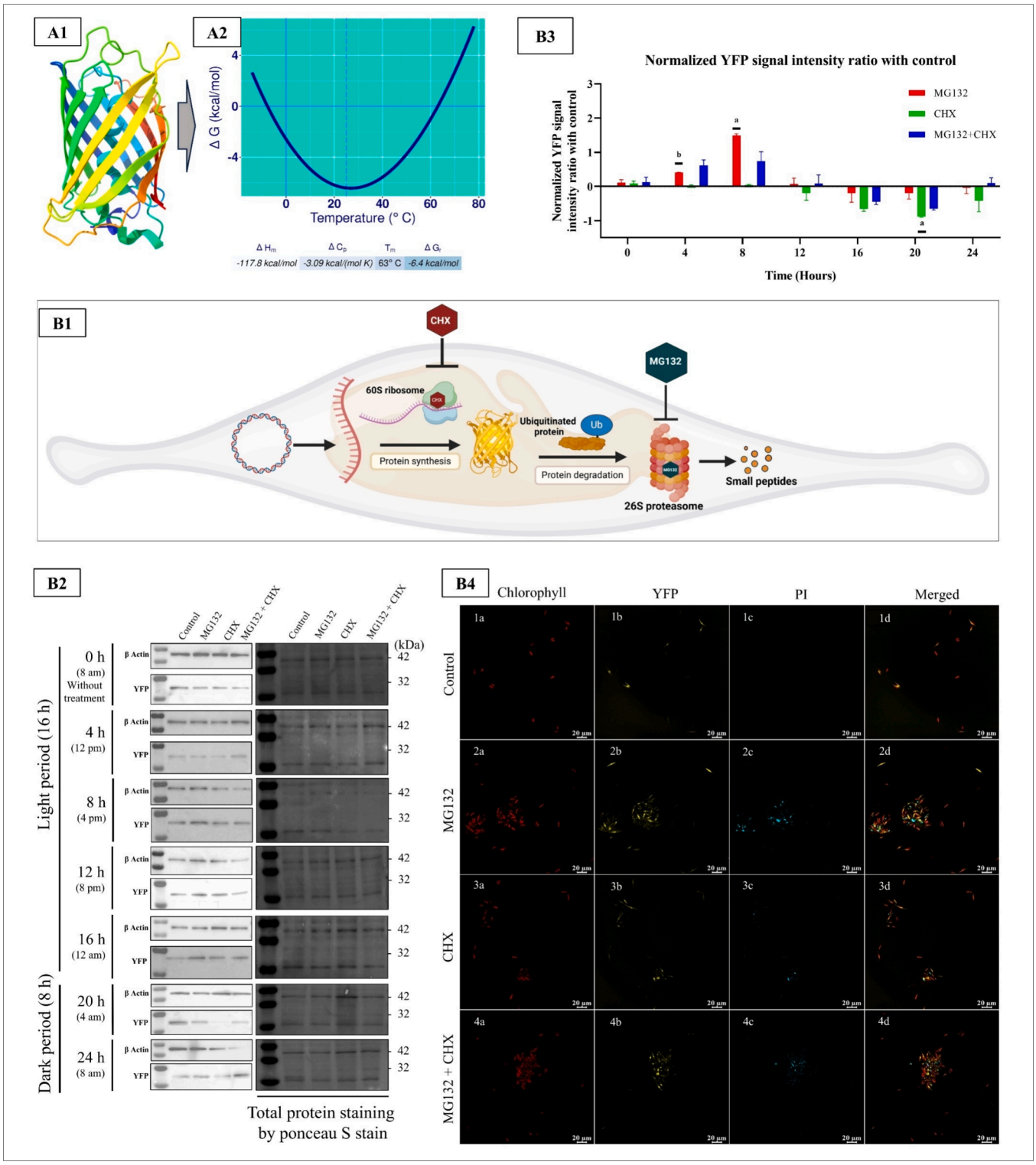

Fig. 4. ***In silico*** **and** ***in vivo*** **stability analysis of yellow fluorescent protein.** (A1) 3D structure of YFP generated from Alphafold2. (A2) Thermal characteristics of the protein predicted using SCooP software. (B1) Graphical representation of protein stability analysis using proteasome (MG132) and protein synthesis inhibitors (CHX). (B2) Time courses immunoblot analysis of YFP signal intensity treating with different inhibitors for 24 h period. From left to right in the blots treating with solvent control (control), proteasome inhibitor (MG132), protein biosynthesis inhibitor (CHX), proteasome and protein biosynthesis inhibitor (MG132 + CHX). One representative result of three independent replicates is shown. (B3) Normalized YFP intensity ratio in the inhibitor- vs control treated samples (n = 3) with β actin as housekeeping protein. Mean value is plotted in the graph with standard error. (B4) Viability of *P. tricornutum* cells after 24 h of treatment following PI staining. (B4.1-4a) chlorophyll fluorescence, (B4.1-4b) YFP fluorescence, (B4.1-4c) fluorescence of PI^{+} cells, and (B4.1-4d) the merged image of all fluorescence filters.

cells (Fig. 4D1-4b) and nonviable cells (PI^+ cells) (Fig. 4D1-4c) in inhibitor treated (after 24 h) culture was visualized using confocal microscopy. The fluorescence image showed *P. tricornutum* cells clumps formation with few PI^+ cells in all the treated conditions as compared to homogeneous culture for control (Fig. 4D1-4d). This observation was consistent with the previous observations by Im et al. (2024).

The ubiquitin–proteasome system (UPS) based protein degradation exists in most eukaryotic cells but has not yet been verified in diatoms. A genome-wide study by Ma et al. (2023) on *P. tricornutum* showed that 18 ubiquitin-conjugating enzymes play pivotal roles in maintaining cellular homeostasis under changing environmental conditions. A recent study by Im et al. (2024) on *P. tricornutum* using MG132, demonstrated the extent of the UPS systems used in the degradation of Aureochromes (PtAUREO1a) blue-light photoreceptors and transcription factors. These studies are consistent with the present results and suggest that the UPS system is active and participates in protein turnover in *P. tricornutum*. The current results implied that the newly synthesized YFP was stable for at least 8 h under normal conditions and remained resistant to degradation for up to 12 h when protein synthesis was blocked, after which degradation prevailed.

Overall, this analysis suggests that culture-related parameters affected the generation of fluorescent proteins at the transcript, translational, maturation, and stability levels. To understand the mechanism underlying the noticeably greater level of protein yield, MFI, and YFP^+ cells in culture under optimum culture conditions, thorough transcriptomic, proteomic, and metabolic flux analyses will be necessary. The optimization YFP may not fully capture the range of challenges associated with more complex genetic engineering scenario involving multiple proteins. However, the current approach could be adapted or expanded for more diverse protein expression studies in *P. tricornutum* or other microalgal systems. Finaly, scaling up of algal systems faces several challenges, including poor light distribution, uneven nutrient and gas exchange, pH fluctuation, and inefficient harvesting of low-density cultures. Addressing these inherent challenges is essential for establishing microalgae as viable and economical hosts for heterologous production.

4. Conclusion

This study uniquely applies RSM to optimize YFP expression in *P. tricornutum*, a model diatom with growing biotechnological relevance. By integrating mathematical modeling and experimental validation, we achieved a 4.2-fold increase in YFP MFI and a 1.8-fold rise in total YFP levels (219 ± 9 μg L^{-1}) without affecting biomass. We also provided the first detailed assessment of YFP degradation kinetics, confirming ubiquitin–proteasome system involvement. These findings propose novel media composition, offer a predictive model for optimizing culture conditions to enhance recombinant protein stability in phototrophic hosts, advance diatoms as biomanufacturing platforms, and lays the foundation for heterologous production.

CRediT authorship contribution statement

Arun Augustine: Writing – review & editing, Writing – original draft, Visualization, Methodology, Investigation, Formal analysis, Data curation, Conceptualization. **Anis Messaabi:** Writing – review & editing, Methodology, Investigation, Data curation, Conceptualization. **Elisa Fantino:** Writing – review & editing, Formal analysis, Data curation. **Natacha Merindol:** Writing – review & editing, Supervision, Data curation. **Fatma Meddeb-Mouelhi:** Writing – review & editing, Project administration. **Isabel Desgagné-Penix:** Writing – review & editing, Supervision, Project administration, Funding acquisition, Conceptualization.

Declaration of competing interest

The authors declare the following financial interests/personal relationships which may be considered as potential competing interests: Isabel Desgagne-Penix reports financial support was provided by Natural Sciences and Engineering Research Council of Canada. Isabel Desgagne-Penix reports financial support was provided by Mitacs Canada. If there are other authors, they declare that they have no known competing financial interests or personal relationships that could have appeared to influence the work reported in this paper.

Acknowledgments

We acknowledge that financial support for this research was funded by the Natural Sciences and Engineering Research Council of Canada through the Alliance program Award No ALLRP 570476-2021 to IDP. Additional support in the form of scholarships to AA, AM, and EF, from Mitacs-Acceleration/ program grants no IT16463 and IT19432 to IDP is also acknowledged. AA acknowledge the valuable support from Prof. Tagnon Missihoun, Ms. Mélodie B. Plourde and other lab members from UQTR. The graphical abstract figure was created with BioRender.com. During the preparation of this work, the authors used ChatGPT 4.0 in order to correct grammatical errors and enhance readability. After using this tool, the authors reviewed and edited the content as needed and take full responsibility for the content of the publication.

Appendix A. Supplementary data

Supplementary data to this article can be found online at https://doi.org/10.1016/j.biortech.2025.132336.

Data availability

Data will be made available on request.

References

Alipanah, L., Rohloff, J., Winge, P., Bones, A.M., Brembu, T., 2015. Whole-cell response to nitrogen deprivation in the diatom *Phaeodactylum tricornutum*. J. Exp. Bot. 66 (20), 6281–6296.

Alipanah, L., Winge, P., Rohloff, J., Najafi, J., Brembu, T., Bones, A.M., 2018. Molecular adaptations to phosphorus deprivation and comparison with nitrogen deprivation responses in the diatom *Phaeodactylum tricornutum*. PLoS One 13 (2), e0193335.

Anderson, M.R., Padgett, C.M., Dargatz, C.J., Nichols, C.R., Vittalam, K.R., DeVore, N.M., 2023. Engineering a yellow thermostable fluorescent protein by rational design. ACS Omega 8 (1), 436–443.

Chávez, M.N., Schenck, T.L., Hopfner, U., Centeno-Cerdas, C., Somlai-Schweiger, I., Schwarz, C., Machens, H.-G., Heikenwalder, M., Bono, M.R., Allende, M.L., Nickelsen, J., Egaña, J.T., 2016. Towards autotrophic tissue engineering: Photosynthetic gene therapy for regeneration. Biomaterials 75, 25–36.

Chen, J., Huang, Y., Shu, Y., Hu, X., Wu, D., Jiang, H., Wang, K., Liu, W., Fu, W., 2022. Recent progress on systems and synthetic biology of diatoms for improving algal productivity. Front. Bioeng. Biotechnol. 10, 908804.

Dayana Priyadharshini, S., Bakthavatsalam, A.K., 2016. Optimization of phenol degradation by the microalga *Chlorella pyrenoidosa* using Plackett-Burman Design and Response Surface Methodology. Bioresour. Technol. 207, 150–156.

De Martino, A., Bartual, A., Willis, A., Meichenin, A., Villazán, B., Maheswari, U., Bowler, C., 2011. Physiological and molecular evidence that environmental changes elicit morphological interconversion in the model diatom *Phaeodactylum tricornutum*. Protist 162 (3), 462–481.

Dehouck, Y., Folch, B., Rooman, M., 2008. Revisiting the correlation between proteins' thermoresistance and organisms' thermophilicity. PEDS 21 (4), 275–278.

Diamond, A., Diaz-Garza, A.M., Li, J., Slattery, S.S., Merindol, N., Fantino, E., Meddeb-Mouelhi, F., Karas, B.J., Barnabé, S., Desgagné-Penix, I., 2023. Instability of extrachromosomal DNA transformed into the diatom *Phaeodactylum tricornutum*. Algal Res. 70, 102998.

Eichler-Stahlberg, A., Weisheit, W., Ruecker, O., Heitzer, M., 2009. Strategies to facilitate transgene expression in *Chlamydomonas reinhardtii*. Planta 229 (4), 873–883.

Erdene-Ochir, E., Shin, B.K., Kwon, B., Jung, C., Pan, C.H., 2019. Identification and characterisation of the novel endogenous promoter HASP1 and its signal peptide from *Phaeodactylum tricornutum*. Sci. Rep. 9 (1).

Fantino, E., Awwad, F., Merindol, N., Diaz Garza, A.M., Gélinas, S.-E., Gajón Robles, G. C., Custeau, A., Meddeb-Mouelhi, F., Desgagné-Penix, I., 2024. Bioengineering *Phaeodactylum tricornutum*, a marine diatom, for cannabinoid biosynthesis. Algal Res. 77, 103379.

Filloramo, G.V., Curtis, B.A., Blanche, E., Archibald, J.M., 2021. Re-examination of two diatom reference genomes using long-read sequencing. BMC Genomics 22 (1), 379.
Gómez-Loredo, A., Benavides, J., Rito-Palomares, M., 2016. Growth kinetics and fucoxanthin production of *Phaeodactylum tricornutum* and *Isochrysis galbana* cultures at different light and agitation conditions. J. Appl. Phycol. 28 (2), 849–860.
Guerra, P., Vuillemenot, L.A., Rae, B., Ladyhina, V., Milias-Argeitis, A., 2022. Systematic *in vivo* characterization of fluorescent protein maturation in budding yeast. ACS Synth. Biol. 11 (3), 1129–1141.
Iizuka, R., Yamagishi-Shirasaki, M., Funatsu, T., 2011. Kinetic study of de novo chromophore maturation of fluorescent proteins. Anal. Biochem. 414 (2), 173–178.
Im, S.H., Madhuri, S., Lepetit, B., Kroth, P.G., 2024. Functional demonstration of Aureochrome 1a proteasomal degradation after blue light incubation in the diatom *Phaeodactylum tricornutum*. J. Plant Physiol. 292, 154148.
Karas, B.J., Diner, R.E., Lefebvre, S.C., McQuaid, J., Phillips, A.P., Noddings, C.M., Brunson, J.K., Valas, R.E., Deerinck, T.J., Jablanovic, J., Gillard, J.T., Beeri, K., Ellisman, M.H., Glass, J.I., Hutchison 3rd, C.A., Smith, H.O., Venter, J.C., Allen, A.E., Dupont, C.L., Weyman, P.D., 2015. Designer diatom episomes delivered by bacterial conjugation. Nat. Commun. 6, 6925.
Kiefer, A.M., Niemeyer, J., Probst, A., Erkel, G., Schroda, M., 2022. Production and secretion of functional SARS-CoV-2 spike protein in *Chlamydomonas reinhardtii*. Front. Plant. Sci. 13, 988870.
Lee, D.H., Goldberg, A.L., 1998. Proteasome inhibitors cause induction of heat shock proteins and trehalose, which together confer thermotolerance in *Saccharomyces cerevisiae*. Mol. Cell. Biol. 18 (1), 30–38.
Leuenberger, P., Ganscha, S., Kahraman, A., Cappelletti, V., Boersema, P.J., von Mering, C., Claassen, M., Picotti, P., 2017. Cell-wide analysis of protein thermal unfolding reveals determinants of thermostability. Science 355 (6327), eaai7825.
Liang, Y., Sun, M., Tian, C., Cao, C., Li, Z., 2014. Effects of salinity stress on the growth and chlorophyll fluorescence of *Phaeodactylum tricornutum* and *Chaetoceros gracilis* (Bacillariophyceae). Bot. Mar. 57 (6), 469–476.
Ma, W., Du, H., Kazmi, S.S.U.H., Chen, J., Chen, W., Fan, Y., Liu, Z., Luo, H., Fang, H., Wang, Z., Liu, X., 2023. UBC gene family and their potential functions on the cellular homeostasis under the elevated pCO_2 stress in the diatom *Phaeodactylum tricornutum*. Ecol. Indicators 148, 110106.
Marter, P., Schmidt, S., Kiontke, S., Moog, D., 2020. Optimized mRuby3 is a suitable fluorescent protein for in vivo co-localization studies with GFP in the diatom *Phaeodactylum tricornutum*. Protist 171 (1), 125715.
Mirdita, M., Schütze, K., Moriwaki, Y., Heo, L., Ovchinnikov, S., Steinegger, M., 2022. ColabFold: making protein folding accessible to all. Nat. Methods 19 (6), 679–682.
Nagai, T., Ibata, K., Park, E.S., Kubota, M., Mikoshiba, K., Miyawaki, A., 2002. A variant of yellow fluorescent protein with fast and efficient maturation for cell-biological applications. Nat. Biotechnol. 20 (1), 87–90.
Nur, M.M.A., Muizelaar, W., Boelen, P., Buma, A.G.J., 2018. Environmental and nutrient conditions influence fucoxanthin productivity of the marine diatom *Phaeodactylum tricornutum* grown on palm oil mill effluent. J. Appl. Phycol. 31 (1), 111–122.
Obrig, T.G., Culp, W.J., McKeehan, W.L., Hardesty, B., 1971. The mechanism by which cycloheximide and related glutarimide antibiotics inhibit peptide synthesis on reticulocyte ribosomes. J. Biol. Chem. 246 (1), 174–181.
Ouyang, Z., Chen, R., Liu, Q., He, L., Cai, W.J., Yin, K., 2018. Biological regulation of carbonate chemistry during diatom growth under different concentrations of Ca^{2+} and Mg^{2+}. Mar. Chem. 203, 38–48.
Pfaffl, M.W., 2001. A new mathematical model for relative quantification in real-time RT–PCR. Nucleic Acids Res. 29 (9), 2002–2007.
Plackett, R.L., Burman, J.P., 1946. The design of optimum multifactorial experiments. Biometrika 33 (4), 305–325.
Pucci, F., Kwasigroch, J.M., Rooman, M., 2017. SCooP: an accurate and fast predictor of protein stability curves as a function of temperature. Bioinformatics 33 (21), 3415–3422.
Rajendran, A., Palanisamy, A., Thangavelu, V., 2008. Evaluation of medium components by Plackett-Burman statistical design for lipase production by *Candida rugosa* and kinetic modeling. Chin. J. Biotechnol. 24 (3), 436–444.
Ramos-Martinez, E.M., Fimognari, L., Sakuragi, Y., 2017. High-yield secretion of recombinant proteins from the microalga *Chlamydomonas reinhardtii*. Plant Biotechnol. J. 15 (9), 1214–1224.
Siaut, M., Heijde, M., Mangogna, M., Montsant, A., Coesel, S., Allen, A., Manfredonia, A., Falciatore, A., Bowler, C., 2007. Molecular toolbox for studying diatom biology in *Phaeodactylum tricornutum*. Gene 406 (1–2), 23–35.
Sivakaminathan, S., Hankamer, B., Wolf, J., Yarnold, J., 2018. High-throughput optimisation of light-driven microalgae biotechnologies. Sci. Rep. 8 (1), 11687.
Slattery, S.S., Giguere, D.J., Stuckless, E.E., Shrestha, A., Briere, L.K., Galbraith, A., Reaume, S., Boyko, X., Say, H.H., Browne, T.S., Frederick, M.I., Lant, J.T., Heinemann, I.U., O'Donoghue, P., Dsouza, L., Martin, S., Howard, P., Jedeszko, C., Ali, K., Styba, G., Flatley, M., Karas, B.J., Gloor, G.B., Edgell, D.R., 2022. Phosphate-regulated expression of the SARS-CoV-2 receptor-binding domain in the diatom *Phaeodactylum tricornutum* for pandemic diagnostics. Sci. Rep. 12 (1), 7010.
Sojikul, P., Buehner, N., Mason, H.S., 2003. A plant signal peptide–hepatitis B surface antigen fusion protein with enhanced stability and immunogenicity expressed in plant cells. PNAS 100 (5), 2209–2214.
Vartanian, M., Desclés, J., Quinet, M., Douady, S., Lopez, P.J., 2009. Plasticity and robustness of pattern formation in the model diatom *Phaeodactylum tricornutum*. New Phytol. 182 (2), 429–442.
Villanova, V., Singh, D., Pagliardini, J., Fell, D., Le Monnier, A., Finazzi, G., Poolman, M., 2021. Boosting biomass quantity and auality by improved mixotrophic culture of the diatom *Phaeodactylum tricornutum*. Front. Plant. Sci. 12, 642199.
Wu, Y., Gao, K., Riebesell, U., 2010. CO_2-induced seawater acidification affects physiological performance of the marine diatom *Phaeodactylum tricornutum*. Biogeosciences 7 (9), 2915–2923.